HHS Public Access

Identification of focally amplified lineage-specific super-enhancers in human epithelial cancers

Xiaoyang Zhang[1,2,*], **Peter S. Choi**[1,2,*], **Joshua M. Francis**[1,2,*], **Marcin Imielinski**[1,2,3], **Hideo Watanabe**[4,5], **Andrew D. Cherniack**[2], and **Matthew Meyerson**[1,2,6,7]

[1]Department of Medical Oncology, Dana-Farber Cancer Institute, Boston, MA 02215, USA

[2]Cancer Program, Broad Institute of Harvard and MIT, Cambridge, MA 02142, USA

[3]Molecular Pathology Unit, Massachusetts General Hospital, Charlestown, MA, 02129, USA

[4]Department of Medicine, Division of Pulmonary, Critical Care and Sleep Medicine, Icahn School of Medicine at Mount Sinai, New York, NY 10029, USA

[5]Department of Genetics and Genomic Sciences, Icahn School of Medicine at Mount Sinai, New York, NY 10029, USA

[6]Department of Pathology, Harvard Medical School, Boston, MA 02115, USA

[7]Center for Cancer Genome Discovery, Dana-Farber Cancer Institute, Boston, MA 02215, USA

Abstract

Whole genome analysis approaches are revealing recurrent cancer-associated somatic alterations in non-coding DNA regions. We combined somatic copy number analysis of 12 tumor types with tissue-specific epigenetic profiling to identify significant regions of focal amplification harboring super-enhancers. Copy-number gains of non-coding regions harboring super-enhancers near *KLF5*, *USP12*, *PARD6B* and *MYC* are associated with over-expression of these cancer-related genes. We show that two distinct focal amplifications of super-enhancers 3′ to *MYC* in lung adenocarcinoma (*MYC*-LASE) and endometrial carcinoma (*MYC*-ECSE), are physically associated with the *MYC* promoter and correlate with *MYC* over-expression. CRISPR/Cas9-mediated repression or deletion of a constituent enhancer within the *MYC*-LASE region led to significant reductions in the expression of *MYC* and its target genes, and to the impairment of anchorage-independent and clonogenic growth, consistent with an oncogenic function. Our results

demonstrate that genomic amplification of super-enhancers represents a common mechanism to activate cancer driver genes in multiple cancer types.

Somatic copy number alterations (SCNAs), including chromosome arm-level copy changes as well as focal amplifications and deletions, are central events in cancer pathogenesis[1–3]. Analysis of focal SCNAs has led to the identification of many critical cancer driver genes[4–8]. However, for focal amplifications and deletions that occur outside of coding regions, the identity of specific targets has remained unclear. Non-coding regions harbor *cis*-regulatory elements, termed enhancers, that are bound by transcription factors and establish lineage-specific expression programs that define cellular identity[9–13]. Enhancers are characterized by the histone modifications H3K4me1 and H3K27ac, binding of coactivators such as p300, and increased chromatin accessibility as defined by DNaseI hypersensitivity[14–19]. Methods such as chromatin immunoprecipitation sequencing (ChIP-seq) and DNaseI hypersensitivity sequencing (DNaseI-seq) have revealed the presence of large clusters of enhancers, termed super-enhancers due to the high level of transcription factor binding associated with these regions[19–25]. Previously, super-enhancers have been implicated in oncogene activation in cancer through focused analyses of individual tumor types[22,26–30]. In this study, we systematically investigate SCNAs of non-coding regions at a pan-cancer scale and provide evidence suggesting that focal amplifications of super-enhancers are a common mechanism for upregulating the expression of cancer driver genes.

Statistical methods such as GISTIC (Genomic Identification of Significant Targets in Cancer)[2,31] have been developed to identify genomic regions that are recurrently amplified or deleted across cancer types. We examined GISTIC analysis of The Cancer Genome Atlas (TCGA) copy number results for 10,534 samples across 29 tumor types, and identified non-coding focal amplification peaks in 19 of these tumor types after filtering out amplicons containing genes in the Reference Sequence (Refseq) database (Fig. 1a and Supplementary Table 1). For 12 out of the 19 tumor types, H3K27ac ChIP-seq data from corresponding tissue or cell lines were available from either public datasets such as ENCODE and the Roadmap Epigenomics project[20–22,32] or from our own collection (Supplementary Table 2). From the 55 focally amplified non-coding regions identified by our analysis, we found six tissue-specific focal amplification peaks harboring super-enhancers as defined by previous criteria[22,25,33] (Fig. 1b).

The six focally amplified super-enhancers reside in four distinct genomic loci. The focal amplification on chr13q identified in head and neck squamous cell carcinoma (HNSC) (~110 kb, chr13:73880690-73990596) and esophageal carcinoma (ESCA) (~162 kb, chr13:73880413-74042621), is located between the Kruppel-like transcription factors, *KLF5* and *KLF12* (Fig. 1c). ChIP-seq profiling of H3K27ac in the HNSC cell line BICR-31 revealed that the focal amplification harbors a cluster of three super-enhancers, which we termed *KLF5*-HNSE (*KLF5* Head and Neck squamous cell carcinoma Super-Enhancers). The expression of *KLF5*, but not *KLF12*, is significantly higher in HNSC tumors with *KLF5*-HNSE amplification, suggesting that *KLF5* is the target gene (Fig. 1c, Supplementary Fig. 1). In total, ~3% (n = 15) of HNSC cases have amplification of *KLF5*-HNSE in the absence of *KLF5* gene amplification (Fig. 1c). Similarly, the ESCA amplicon also harbors a

super-enhancer based on the H3K27ac ChIP-seq profile of esophageal cells and ESCA tumors with this amplicon exhibited a trend towards increased *KLF5* expression (Supplementary Fig. 2). In lung adenocarcinomas and lung squamous cell carcinomas, *KLF5* is also significantly mutated with recurrent missense alterations (Campbell *et. al.*, in preparation). These results suggest that *KLF5* is a putative oncogene which can be upregulated in tumors by super-enhancer amplification.

Additional focal amplification peaks on chr13q in colorectal carcinoma (CRC) (~21 kb, chr13:27523026-27544353) and chr20q in liver hepatocellular carcinoma (LIHC) (~22kb chr20:48997377-49019434) were identified. ChIP-seq profiling of H3K27ac in colon crypt cells[32] and in the hepatocellular carcinoma cell line HepG2[20] revealed that these amplicons contain super-enhancers (Fig. 1d,e). CRC tumors containing the chr13q amplicon exhibited significantly higher expression of the nearest gene, ubiquitin specific peptidase 12, *USP12*, a deubiquitinating enzyme implicated in prostate cancer[34] (Fig. 1d and Supplementary Fig. 1). In LIHC tumors with the chr20q amplicon, the expression of the second nearest gene *PARD6B*, rather than the closest gene *PTPN1*, is upregulated, suggesting that *PARD6B* is the target gene (Fig. 1e and Supplementary Fig. 1). PARD6B is part of an intracellular signaling complex involved in cellular polarity; its over-expression may lead to dysregulation of cell orientation and cellular transformation[35].

Frequent non-coding amplifications were identified near the *MYC* gene, with two distinct focal amplification peaks situated ~450 and ~800 kb 3′ to the *MYC* oncogene in lung adenocarcinoma (LUAD) and uterine corpus endometrial carcinoma (UCEC), respectively (Fig. 2a). These peaks are distinct from focally amplified super-enhancer regions ~1.5 Mb and ~1.7 Mb 3′ to *MYC* previously identified in T-cell acute lymphoblastic leukemia (T-ALL) and acute myeloid leukemia (AML), respectively[26,30]. The lung adenocarcinoma peak (chr8:129166547-129190290) encompasses a 23 kb non-coding region that is part of a super-enhancer as defined by the H3K27ac ChIP-seq profile from A549 lung adenocarcinoma cells, which we refer to as *MYC*-LASE (*MYC* Lung Adenocarcinoma Super-Enhancer). In total, ~17% of lung adenocarcinoma cases (n = 86) have a focal amplification of *MYC*-LASE that is co-amplified with *MYC*, while ~2% (n = 11) of cases have a focal amplification of *MYC*-LASE without concurrent amplification of *MYC* (Fig. 2a). Four out of 52 (~8%) lung adenocarcinoma cell lines profiled for copy-number alterations by the Cancer Cell Line Encyclopedia (CCLE) project[36] also have focal amplification of *MYC*-LASE in the absence of *MYC* amplification (Supplementary Fig. 3). Rearrangement analysis of whole genome sequencing data from 70 lung adenocarcinoma tumor/normal pairs[6,37] revealed two tumors with somatic focal amplification of *MYC*-LASE occurring as a tandem duplication event (Fig. 2b). We performed H3K27ac ChIP-seq in two additional lung adenocarcinoma cell lines, NCI-H2009 and NCI-H358, the lung squamous cell carcinoma (LUSC) line HCC95 and the small cell lung carcinoma (SCLC) cell line NCI-H2171 and validated that *MYC*-LASE is part of a lung adenocarcinoma-specific super-enhancer (Fig. 2c and Supplementary Fig. 3).

The endometrial carcinoma peak (chr8:129543949-129554294) encompasses a 10 kb non-coding region that harbors a super-enhancer as defined by the H3K27ac ChIP-seq profile of the endometrial carcinoma cell line Ishikawa (Fig. 2d), and which we refer to as *MYC-*

ECSE (*MYC* Endometrial carcinoma Super-Enhancer). Approximately 10% of cases (n = 54) have focal amplification of both *MYC*-ECSE and *MYC*, while ~4% (n = 20) of cases have focal amplification of only *MYC*-ECSE (Fig. 2a). The H3K27ac and p300 ChIP-seq profiles of *MYC*-LASE and *MYC*-ECSE indicate that each super-enhancer is active only in cell lines from each respective tumor type (Fig. 2c–d and Supplementary Fig. 4).

Distal enhancers regulate target gene expression through chromatin loops that connect enhancers with target gene promoters[38–40]. We performed chromosome conformation capture (3C) assays in A549 and Ishikawa cells and found that *MYC*-LASE physically interacts with the *MYC* promoter only in A549 cells, and reciprocally, that *MYC*-ECSE physically interacts with the *MYC* promoter only in Ishikawa cells (Fig. 2e). In addition, tumors with amplification of *MYC* alone or *MYC*-LASE/ECSE alone have higher *MYC* expression than tumors lacking either amplification (Fig. 2f). These results suggest that both *MYC*-LASE and *MYC*-ECSE drive *MYC* expression through lineage-specific chromatin loops.

To determine if copy number gain of super-enhancers drives oncogene expression and tumorigenesis, we focused on *MYC*-LASE. The binding profile for p300, a marker for enhancer activity[14], revealed five constituent enhancers (e1–e5) within *MYC*-LASE in A549 and NCI-H2009 cells, which overlap with H3K27ac enrichment and DNase I hypersensitivity (Fig. 3a). Among the five constituent enhancers, the e3 enhancer is associated with the highest p300 binding as well as the greatest DNase I hypersensitivity (Fig. 3a). In luciferase reporter assays in A549, NCI-H358 and NCI-H2009 cells, the e3 enhancer was also found to have the strongest activity (Fig. 3b). In contrast, *MYC*-LASE has no detectable enhancer activity in HEK293 cells, confirming that this super-enhancer is specific to lung adenocarcinoma (Supplementary Fig 5). Duplication of the e3 enhancer in the luciferase reporter construct resulted in >2-fold higher luciferase expression relative to a single copy of e3, demonstrating that an increase in copy number of the enhancer region may upregulate target gene expression (Fig. 3c).

We next aimed to identify the transcription factors that are required for lung adenocarcinoma-specific activity of the e3 enhancer. We tested ~350 bp fragments of the ~1.5kb e3 region in luciferase reporter assays and discovered that a minimal ~148bp region (mini-e3) was responsible for the preponderance of e3 enhancer activity (Fig. 4a). Transcription factor motif analysis using the ENCODE motif dataset[41] identified GATA3, FOXA1, NFE2L2 and CEBPB as candidate factors capable of binding to mini-e3 (Fig. 4b). Deletion of specific transcription factor binding motif sequences within mini-e3 demonstrated that the NFE2L2 and CEBPB motifs were necessary to maintain maximal e3 enhancer activity (Fig. 4c). Short interfering RNA (siRNA)-mediated knockdown of NFE2L2 and CEBPB in A549 cells led to a significant reduction in e3-driven luciferase reporter activity as compared to control siRNAs (Fig. 4d and Supplementary Fig. 6). The binding of NFE2L2 and CEBPB to the super-enhancer was subsequently confirmed by ChIP-seq, with greatest enrichment at the e3 constituent enhancer (Fig. 4e).

To investigate the functional role of the amplified e3 enhancer region, we first targeted catalytically inactive Cas9 (dCas9) fused to the Kruppel-associated box (KRAB)

transcriptional repressor domain[42,43] to inhibit e3 enhancer activity in NCI-H2009 lung adenocarcinoma cells that contain four copies of *MYC*-LASE. Targeting KRAB-dCas9 to the e3 enhancer using two independent single guide RNAs (sgRNAs) resulted in a marked decrease in H3K27ac, compared to cells expressing a control non-targeting sgRNA or KRAB-dCas9 only (Fig. 5a). A significant reduction (~50%) of *MYC* gene expression was also observed after KRAB-dCas9 mediated repression, confirming *MYC* as a target gene of the e3 enhancer (Fig. 5b and Supplementary Fig. 7). Furthermore, comparison of RNA sequencing (RNA-seq) data with gene expression signatures[44–47] for *MYC* using Gene Set Enrichment Analysis (GSEA)[48] revealed that e3 enhancer repression is associated with a significant decrease in the expression of MYC target genes (Fig. 5c). Finally, repression of the e3 enhancer led to a significant decrease in both anchorage-independent and clonogenic growth (Fig. 5d and 5e; Supplementary Fig. 8), demonstrating that activity of the e3 enhancer is critical for the tumorigenicity of lung adenocarcinoma cells.

We also used the CRISPR/Cas9 system to specifically delete the e3 enhancer in NCI-H2009 cells. Two independent pairs of sgRNAs were used to target Cas9 to the boundaries of the e3 enhancer. Deletion of e3 was detected by PCR in cells transduced with either pair of e3-targeting sgRNAs, but not in cells transduced with a pair of non-targeting sgRNAs (Fig. 6a–c). Deletion of the e3 enhancer region resulted in a ~30% reduction in *MYC* expression (Fig. 6d) and a significant impairment of both anchorage-independent and clonogenic growth (Fig. 6e and 6f; Supplementary Fig. 9). These results suggest that copy number gain of the e3 enhancer region drives *MYC* over-expression, which contributes to the tumorigenic phenotype.

MYC overexpression has been observed as a consequence of rearrangements with the IgH locus in Burkitts lymphoma[22,49] (Fig. 6g, lower left diagram) as well as through amplifications of the *MYC* gene itself in several tumor types[2] (Fig. 6g, lower left middle diagram). Similar to our findings, focal amplification of different super-enhancer regions downstream of *MYC* have been reported in T-ALL and AML[26,30]. Collectively, these data suggest that copy number gain of super-enhancers is highly lineage-specific but may be a common mechanism for upregulating *MYC* expression in diverse types of cancer (Fig. 6g, lower right panel).

Chromosomal rearrangements that result in the placement of a super-enhancer adjacent to an oncogene have been described in multiple myeloma, leukemia, medulloblastoma and glioblastoma[22,27,29,50]. Here, we systematically investigate another somatic structural alteration – focal copy number amplification – through pan-cancer analysis of 10,534 tumors integrating genomic, epigenomic and transcriptomic data. We report six super-enhancer regions to be focally amplified across different cancer types. These super-enhancer amplifications are associated with over-expression of the *MYC* oncogene as well as the *KLF5*, *USP12* and *PARD6B* genes. Thus, focal amplification of super-enhancers represents a new class of structural alterations with functional implications in cancer. Further identification and characterization of these events through whole-genome and long-read sequencing approaches may shed insight into mechanisms of tumorigenesis and provide novel targets for therapeutic intervention.

Online methods

Pan-Cancer copy number alteration analysis

GISTIC analyses were performed in 29 tumor types (Supplementary Table 1), using copy number data from version 3.0 of the SNP pipeline on 22-Oct-2014 from TCGA copy number portal[2,31]. Focal amplification peaks of non-coding regions were found in 19 tumor types of which 12 tumor types had H3K27ac ChIP-seq data available for the relevant tissue type (Supplementary Table 1 and 2).

Cell lines

BICR-31 was obtained from Sigma-Aldrich, and A549, NCI-H2009, NCI-H358, HCC95, and Ishikawa cells were obtained from the American Type Culture Collection. Cells were cultured in RPMI 1640 medium supplemented with 10% FBS and 1% penicillin-streptomycin.

ChIP-seq

Chromatin-immunoprecipitation followed by massive parallel sequencing (ChIP-seq) was performed as previously described[51,52]. Briefly, cells were first crosslinked and lysed. The chromatin extract was sonicated using a Diagenode bioruptor and immunoprecipitated with an anti-H3K27ac antibody (Abcam, ab4729). DNA was extracted and processed with the NEB ChIP-seq library prep kit (E6200S) and sequenced on an Illumina MiSeq (50bp single-end). Sequence reads were aligned to hg19 genome by BWA[53] and H3K27ac binding sites were called by MACS[54]. ChIP-seq was done in duplicate and the results were uploaded to the Gene Expression Omnibus (GSE66992). ChIP-seq data from public datasets are listed in Supplementary Table 2.

RNA-seq

RNA was extracted using the Qiagen RNeasy kit with on-column DNase I treatment. 1 ug of RNA for each sample was processed with the NEBNext PolyA mRNA Magnetic Isolation Module (NEB #E7490) and further processed with the NEBNext Ultra Directional RNA Library Prep Kit (NEB #E7420S). RNA libraries were then sequenced on an Illumina MiSeq (75bp paired-end). Sequence reads were aligned using the PRADA pipeline and differential gene expression was called using the Cufflinks pipeline. RNA-seq was done in duplicate and the results were uploaded to the Gene Expression Omnibus (GSE72001).

Super enhancer identification

Super enhancers were called from the ROSE pipeline[24,55] using H3K27ac ChIP-seq data including aligned reads and binding sites called from MACS. Briefly, enhancers were first clustered based on their distance to each other, and then super-enhancers were identified based on the enrichment of the H3K27ac ChIP-seq signal of each enhancer cluster.

Luciferase reporter assays

The pGL3 promoter luciferase reporter system (Promega) was used. The enhancer regions were cloned upstream of the pGL3 minimal promoter region using MluI and XhoI restriction

enzyme sites. The enhancer luciferase constructs were then co-transfected with a control Renilla luciferase construct into cells using Fugene 6 (Promega). The luciferase signal was first normalized to the Renilla luciferase signal and then normalized to the signal from the empty pGL3 plasmid. Primers used for cloning are listed in Supplementary Table 3.

3C-qPCR

Chromosome conformation capture (3C) assays were performed as previously described[52,56]. 3C ligation products were quantified by SYBR-green based PCR. BAC libraries (RP11-628C14, RP11-55J15, CTD-2034C18, RP11-69H6 and CTD-2218N24) containing DNA fragments covering the tested regions were used as template controls for normalizing digestion, ligation and primer efficiency. 3C primers and genomic coordinates of their targets are listed in Supplementary Table 3.

Site-directed deletion of motif sequence

The QuikChange Lightning site-directed mutagenesis system (Agilent Technologies Inc.) was used to generate deletions of the predicted motif sequences in the e3 region. Primers used are listed in Supplementary Table 3.

CRISPR/Cas9 mediated repression and deletion of the enhancer region

CRISPR/Cas9 single-guide RNAs (sgRNA) were identified using the MIT CRISPR Design tool and control non-targeting sgRNAs were selected from the GeCKOv2 library[57]. All sgRNA sequences are listed in Supplementary Table 3. For repression of the e3 enhancer, the KRAB-dCas9 fusion gene was PCR amplified from pHR-SFFV-KRAB-dCas9-P2A-mCherry (Addgene #60954) and cloned into the XbaI/BamHI sites of lentiCas9-blast (Addgene #52962) to generate lenti-KRAB-dCas9-blast. SgRNAs were cloned into lentiGuide-Puro (Addgene #52963). NCI-H2009 cells were first infected with lenti-KRAB-dCas9-blast and selected with 6μg/ml of blasticidin. Cells stably expressing KRAB-dCas9 were then subsequently infected with sgRNAs and selected with 2μg/ml puromycin. For deletion of the e3 enhancer, tandem U6-promoter-sgRNA and H1-promoter-sgRNA cassettes were cloned into lentiCRISPR_v2 (Addgene #60954) for single vector expression of two sgRNAs as follows: 1) U6-sgRNA and H1-sgRNA products were generated by PCR amplification using the primers listed in Supplementary Table 3, 2) PCR products were then digested with BsmBI to generate compatible sticky ends, 3) finally, three-way ligation of the two PCR products and BsmBI-digested lentiCRISPR_v2 was performed using T7 DNA ligase (NEB #M0318). Control 'empty' lentiCRISPR_v2 lacking expression of any sgRNAs was generated by BsmBI digestion, followed by blunting of ends (NEB #E1201) and ligation with T4 DNA ligase (NEB #M0202). After infection, cells were selected with 2μg/ml of puromycin. To detect deletion of the e3 enhancer, genomic DNA was first extracted using QuickExtract DNA extraction solution (Epicentre #QE09050) and then used for PCR using Q5 high-fidelity DNA polymerase (NEB #M0491) with the primers listed in Supplementary Table 3.

Anchorage-independent and clonogenic growth assays

To measure anchorage-independent growth, a base layer of 2ml of 0.75% select agar in RPMI/10% FBS was first prepared in each well of a 6-well plate. Cells were then plated in 1ml of a top layer of 0.3% select agar in RPMI/10% FBS. After 2 weeks, wells were photographed and colonies were counted using CellProfiler software. For the clonogenic growth assay, approximately 300 cells were seeded in 2ml of RPMI/10% FBS in each well of a 6-well plate. Media was completely refreshed every 7 days. Cells were fixed with 100% methanol and then stained with 0.5% crystal violet in 25% methanol. Wells were destained using 10% acetic acid and the crystal-violet signal was read at 595 nm on a Spectramax spectrophotometer.

TaqMan gene expression assay

Quantitative PCR was performed in duplicate using the TaqMan Universal PCR Mastermix on an ABI Quantstudio 6 instrument. The following premade 5′ nuclease assays were ordered from Integrated DNA Technologies: MYC (Hs.PT.58.26770695), NCL (Hs.PT. 58.1260587), CDK4 (Hs.PT.58.584267), ODC1 (Hs.PT.58.27029915), NPM1 (Hs.PT. 58.40019160) and internal reference HPRT1 (Hs.PT.58v.45621572). Relative expression levels were calculated using the   Ct method.

siRNA-directed gene silencing

A549 cells were transfected with scrambled siRNA (siNC), siNFE2L2 or siCEBPB using Lipofectamine RNAiMAX (Life Technologies). RNA was extracted 48 hours after transfection using the Qiagen RNeasy Kit with on-column DNase treatment. Pre-verified Silencer Select siRNAs (Life Technologies, s9491 and s9492 for NFE2L2, and s2891 and s2892 for CEBPB) were used. To assess the effect of siRNAs, western-blot was performed using antibodies against NFE2L2 (Abcam ab62352), CEBPB (Santa Cruz sc-150) and β-ACTIN (Cell signaling #3700).

Public data usage

Accession numbers for ENCODE data, the Roadmap project data and other public datasets used in this study are listed in Supplementary Table 2.

Supplementary Material

Refer to Web version on PubMed Central for supplementary material.

Acknowledgments

References

1. Stratton MR, Campbell PJ, Futreal PA. The cancer genome. Nature. 2009; 458:719–724. [PubMed: 19360079]

2. Beroukhim R, et al. The landscape of somatic copy-number alteration across human cancers. Nature. 2010; 463:899–905. [PubMed: 20164920]

3. Bignell GR, et al. Signatures of mutation and selection in the cancer genome. Nature. 2010; 463:893–898. [PubMed: 20164919]

4. Stephens PJ, et al. Complex landscapes of somatic rearrangement in human breast cancer genomes. Nature. 2009; 462:1005–1010. [PubMed: 20033038]

5. Weir BA, et al. Characterizing the cancer genome in lung adenocarcinoma. Nature. 2007; 450:893–898. [PubMed: 17982442]

6. The Cancer Genome Atlas Research Network. Comprehensive molecular profiling of lung adenocarcinoma. Nature. 2014; 511:543–550. [PubMed: 25079552]

7. Cancer Genome Atlas Research Network. Comprehensive genomic characterization of squamous cell lung cancers. Nature. 2012; 489:519–525. [PubMed: 22960745]

8. Xue W, et al. A cluster of cooperating tumor-suppressor gene candidates in chromosomal deletions. Proc Natl Acad Sci. 2012; 109:8212–8217. [PubMed: 22566646]

9. Ong CT, Corces VG. Enhancer function: new insights into the regulation of tissue-specific gene expression. Nat Rev Genet. 2011; 12:283–293. [PubMed: 21358745]

10. Graf T, Enver T. Forcing cells to change lineages. Nature. 2009; 462:587–594. [PubMed: 19956253]

11. Xie W, Ren B. Enhancing Pluripotency and Lineage Specification. Science. 2013; 341:245–247. [PubMed: 23869010]

12. Bulger M, Groudine M. Functional and Mechanistic Diversity of Distal Transcription Enhancers. Cell. 2011; 144:327–339. [PubMed: 21295696]

13. Lupien M, et al. FoxA1 translates epigenetic signatures into enhancer driven lineage-specific transcription. Cell. 2008; 132:958–970. [PubMed: 18358809]

14. Visel A, et al. ChIP-seq accurately predicts tissue-specific activity of enhancers. Nature. 2009; 457:854–858. [PubMed: 19212405]

15. Heintzman ND, et al. Distinct and predictive chromatin signatures of transcriptional promoters and enhancers in the human genome. Nat Genet. 2007; 39:311–318. [PubMed: 17277777]

16. Heintzman ND, et al. Histone modifications at human enhancers reflect global cell type-specific gene expression. Nature. 2009; 459:108–112. [PubMed: 19295514]

17. Creyghton MP, et al. Histone H3K27ac separates active from poised enhancers and predicts developmental state. Proc Natl Acad Sci. 2010; 107:21931–21936. [PubMed: 21106759]

18. Ernst J, et al. Mapping and analysis of chromatin state dynamics in nine human cell types. Nature. 2011; 473:43–49. [PubMed: 21441907]

19. Thurman RE, et al. The accessible chromatin landscape of the human genome. Nature. 2012; 489:75–82. [PubMed: 22955617]

20. The ENCODE Project Consortium. An integrated encyclopedia of DNA elements in the human genome. Nature. 2012; 489:57–74. [PubMed: 22955616]

21. Roadmap Epigenomics Consortium. et al. Integrative analysis of 111 reference human epigenomes. Nature. 2015; 518:317–330. [PubMed: 25693563]

22. Hnisz D, et al. Super-enhancers in the control of cell identity and disease. Cell. 2013; 155:934–947. [PubMed: 24119843]

23. Pott S, Lieb JD. What are super-enhancers? Nat Genet. 2015; 47:8–12. [PubMed: 25547603]

24. Lovén J, et al. Selective inhibition of tumor oncogenes by disruption of super-enhancers. Cell. 2013; 153:320–334. [PubMed: 23582323]

25. Lovén J, et al. Selective inhibition of tumor oncogenes by disruption of super-enhancers. Cell. 2013; 153:320–334. [PubMed: 23582323]

26. Shi J, et al. Role of SWI/SNF in acute leukemia maintenance and enhancer-mediated Myc regulation. Genes Dev. 2013; doi: 10.1101/gad.232710.113

27. Northcott PA, et al. Enhancer hijacking activates GFI1 family oncogenes in medulloblastoma. Nature. 2014; 511:428–434. [PubMed: 25043047]

28. Mansour MR, et al. An oncogenic super-enhancer formed through somatic mutation of a noncoding intergenic element. Science. 2014; 346:1373–1377. [PubMed: 25394790]

29. Gröschel S, et al. A Single Oncogenic Enhancer Rearrangement Causes Concomitant EVI1 and GATA2 Deregulation in Leukemia. Cell. 2014; 157:369–381. [PubMed: 24703711]

30. Herranz D, et al. A NOTCH1-driven MYC enhancer promotes T cell development, transformation and acute lymphoblastic leukemia. Nat Med. advance online publication, 2014.

31. Mermel CH, et al. GISTIC2.0 facilitates sensitive and confident localization of the targets of focal somatic copy-number alteration in human cancers. Genome Biol. 2011; 12:R41. [PubMed: 21527027]

32. Akhtar-Zaidi B, et al. Epigenomic enhancer profiling defines a signature of colon cancer. Science. 2012; 336:736–739. [PubMed: 22499810]

33. Whyte WA, et al. Master transcription factors and mediator establish super-enhancers at key cell identity genes. Cell. 2013; 153:307–319. [PubMed: 23582322]

34. Burska UL, et al. Deubiquitinating enzyme Usp12 is a novel co-activator of the androgen receptor. J Biol Chem. 2013; 288:32641–32650. [PubMed: 24056413]

35. Qiu RG, Abo A, Martin GS. A human homolog of the C. elegans polarity determinant Par-6 links Rac and Cdc42 to PKCζ signaling and cell transformation. Curr Biol. 2000; 10:697–707. [PubMed: 10873802]

36. Barretina J, et al. The Cancer Cell Line Encyclopedia enables predictive modelling of anticancer drug sensitivity. Nature. 2012; 483:603–607. [PubMed: 22460905]

37. Imielinski M, et al. Mapping the hallmarks of lung adenocarcinoma with massively parallel sequencing. Cell. 2012; 150:1107–1120. [PubMed: 22980975]

38. Kagey MH, et al. Mediator and cohesin connect gene expression and chromatin architecture. Nature. 2010; 467:430–435. [PubMed: 20720539]

39. Deng W, et al. Controlling long-range genomic interactions at a native locus by targeted tethering of a looping factor. Cell. 2012; 149:1233–1244. [PubMed: 22682246]

40. Bailey SD, et al. ZNF143 provides sequence specificity to secure chromatin interactions at gene promoters. Nat Commun. 2015; 2

41. Wang J, et al. Sequence features and chromatin structure around the genomic regions bound by 119 human transcription factors. Genome Res. 2012; 22:1798–1812. [PubMed: 22955990]

42. Gilbert LA, et al. CRISPR-Mediated Modular RNA-Guided Regulation of Transcription in Eukaryotes. Cell. 2013; 154:442–451. [PubMed: 23849981]

43. Kearns NA, et al. Functional annotation of native enhancers with a Cas9-histone demethylase fusion. Nat Methods. 2015; 12:401–403. [PubMed: 25775043]

44. Schlosser I, et al. Dissection of transcriptional programmes in response to serum and c-Myc in a human B-cell line. Oncogene. 2005; 24:520–524. [PubMed: 15516975]

45. Coller HA, et al. Expression analysis with oligonucleotide microarrays reveals that MYC regulates genes involved in growth, cell cycle, signaling, and adhesion. Proc Natl Acad Sci U S A. 2000; 97:3260–3265. [PubMed: 10737792]

46. Zeller KI, Jegga AG, Aronow BJ, O'Donnell KA, Dang CV. An integrated database of genes responsive to the Myc oncogenic transcription factor: identification of direct genomic targets. Genome Biol. 2003; 4:R69. [PubMed: 14519204]

47. Schuhmacher M, et al. The transcriptional program of a human B cell line in response to Myc. Nucleic Acids Res. 2001; 29:397–406. [PubMed: 11139609]

48. Subramanian A, et al. Gene set enrichment analysis: a knowledge-based approach for interpreting genome-wide expression profiles. Proc Natl Acad Sci U S A. 2005; 102:15545–15550. [PubMed: 16199517]

49. Battey J, et al. The human c-myc oncogene: structural consequences of translocation into the IgH locus in Burkitt lymphoma. Cell. 1983; 34:779–787. [PubMed: 6414718]

50. Francis JM, et al. EGFR variant heterogeneity in glioblastoma resolved through single-nucleus sequencing. Cancer Discov. 2014; 4:956–971. [PubMed: 24893890]

51. Cowper-Sal·lari R, et al. Breast cancer risk-associated SNPs modulate the affinity of chromatin for FOXA1 and alter gene expression. Nat Genet. 2012; 44:1191–1198. [PubMed: 23001124]

52. Zhang X, Cowper-Sal lari R, Bailey SD, Moore JH, Lupien M. Integrative functional genomics identifies an enhancer looping to the SOX9 gene disrupted by the 17q24.3 prostate cancer risk locus. Genome Res. 2012; 22:1437–1446. [PubMed: 22665440]

53. Li H, Durbin R. Fast and accurate short read alignment with Burrows-Wheeler transform. Bioinforma Oxf Engl. 2009; 25:1754–1760.

54. Zhang Y, et al. Model-based Analysis of ChIP-Seq (MACS). Genome Biol. 2008; 9:R137. [PubMed: 18798982]

55. Hnisz D, et al. Super-Enhancers in the Control of Cell Identity and Disease. Cell. 2013; 155:934–947. [PubMed: 24119843]

56. Bailey SD, et al. ZNF143 provides sequence specificity to secure chromatin interactions at gene promoters. Nat Commun. 2015; 2

57. Sanjana NE, Shalem O, Zhang F. Improved vectors and genome-wide libraries for CRISPR screening. Nat Methods. 2014; 11:783–784. [PubMed: 25075903]
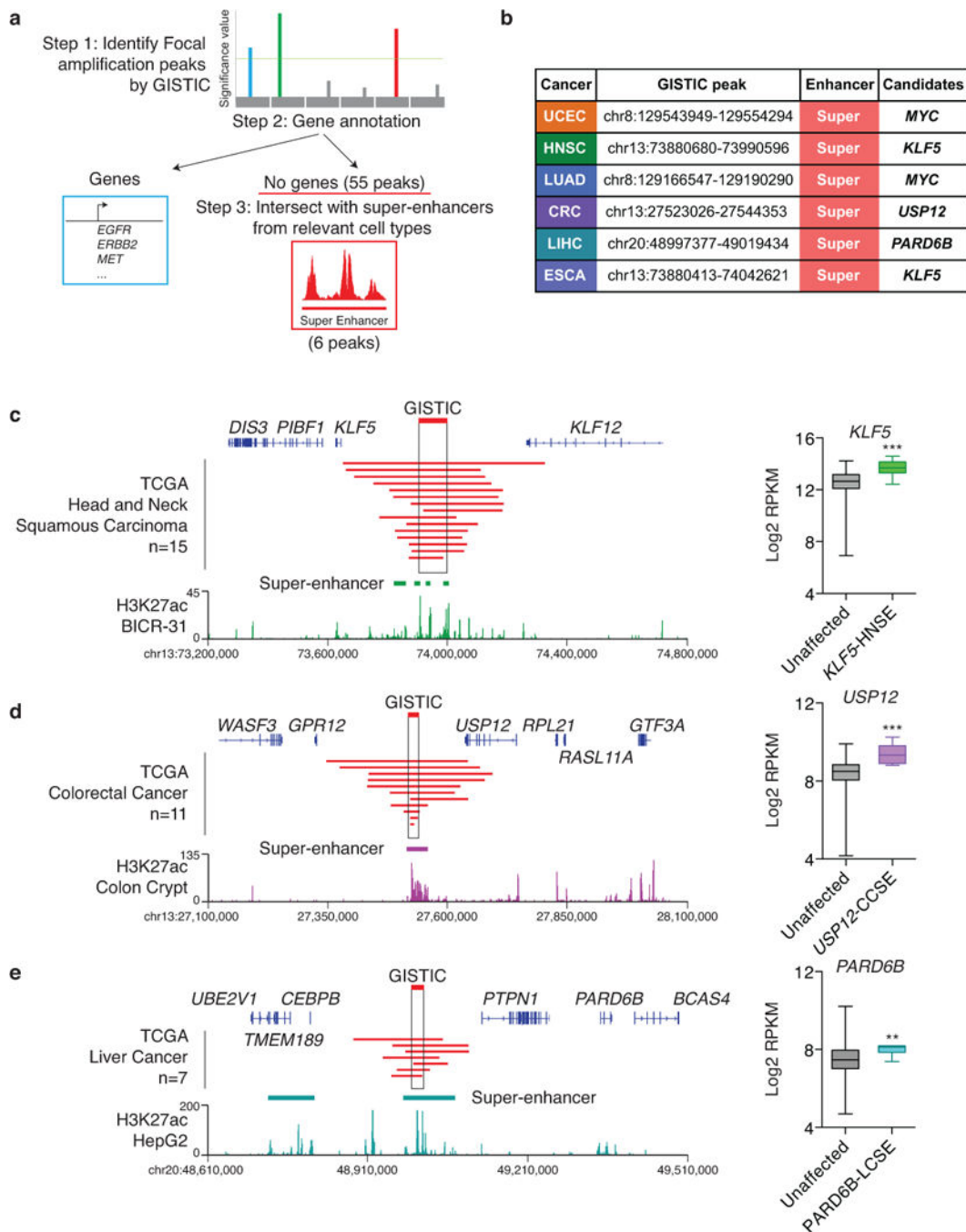
Fig. 1. Pan-cancer analysis identifying focally amplified super-enhancers
(a) Schematic flow chart of pan-cancer GISTIC analysis of 10,534 tumors from 29 tumor types identifying non-coding focal amplifications of super-enhancers. (b) List of non-coding focal amplification regions harboring super-enhancers. UCEC: uterine corpus endometrial carcinoma, HNSC: head and neck squamous cell carcinoma, LUAD: lung adenocarcinoma, CRC: colorectal carcinoma, LIHC: liver hepatocellular carcinoma, CESC: cervical squamous cell carcinoma, ESCA: esophageal carcinoma. (c) The focal amplification on chr13q identified in HNSC. ChIP-seq profile of H3K27ac and super-enhancer regions from

the HNSC cell line BICR-31. Log2 transformed expression level (RPKM) of *KLF5* in HNSC tumors with focal amplification of *KLF5*-HNSE alone (n = 14) and tumors without the amplification (n = 288). Box plot: Middle bar, median; lower and upper box limits, 25th and 75th percentiles, respectively; whiskers, min and max. The *P*-value is derived from a t-test; (**) *p* 0.01; (***) *p* 0.001. **(d)** The focal amplification region on chr13q identified in CRC. ChIP-seq profile of H3K27ac and super-enhancer regions from colon crypt[32]. Log2 transformed expression level (RPKM) of *USP12* in CRC tumors with focal amplification of *USP12*-CCSE alone (n = 6) and tumors without the amplification (n = 127). **(e)** The focal amplification on chr20q identified in LIHC. ChIP-seq profile of H3K27ac and super-enhancer regions from the LIHC cell line HepG2. Log2 transformed expression level (RPKM) of *PARD6B* in LIHC tumors with focal amplification of *PARD6B*-LCSE alone (n = 7) and tumors without the amplification (n = 245).
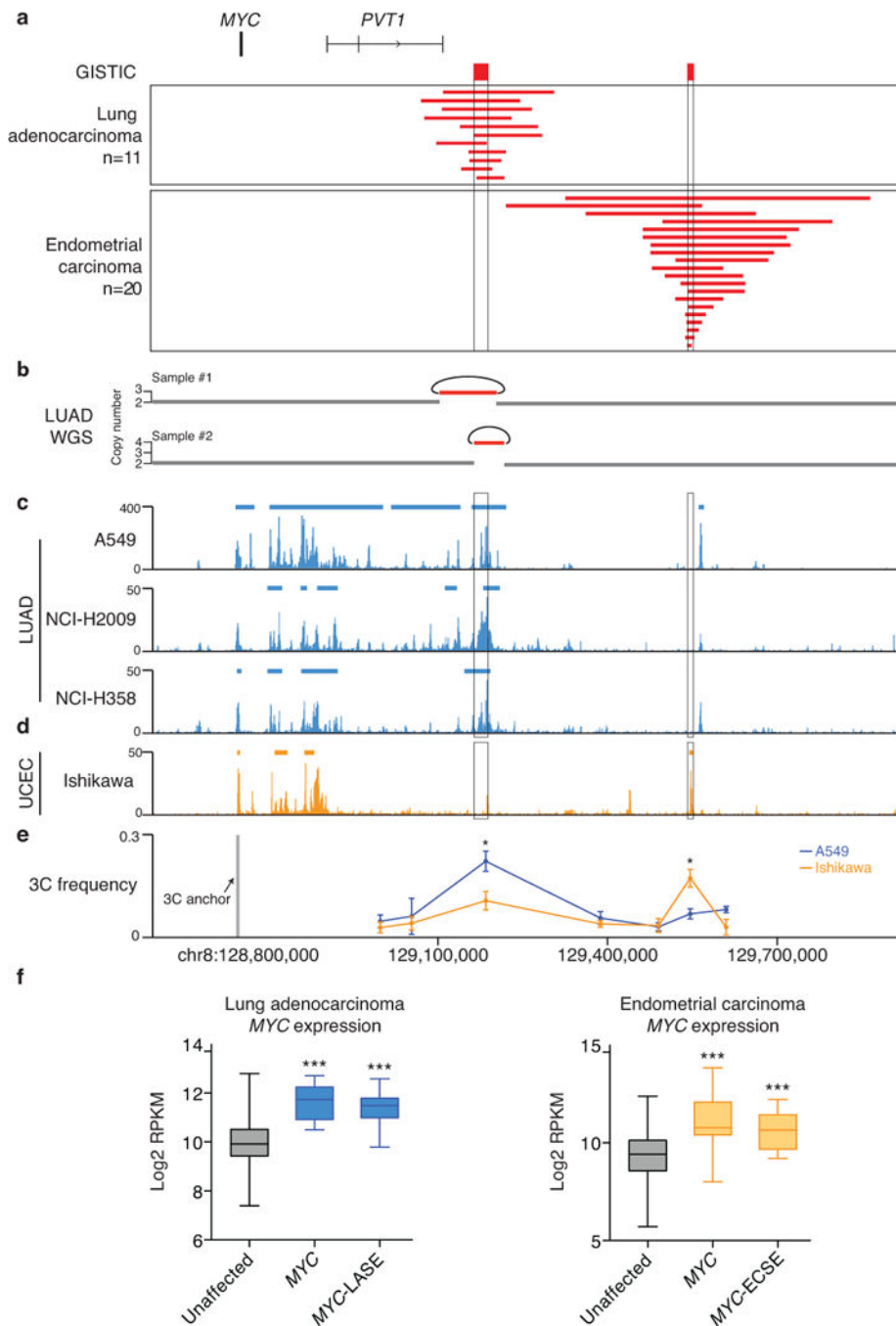
Fig. 2. Lineage-specific focal amplification of super-enhancers adjacent to the *MYC* gene
(a) Focal amplification peaks adjacent to *MYC* identified by GISTIC in lung adenocarcinoma (n = 11/515) and UCEC (n = 20/539). **(b)** Whole genome sequencing rearrangement analysis of two lung adenocarcinomas reveals tandem duplications, indicated by the curves. H3K27ac ChIP-seq profile and super-enhancer regions of the LUAD cell lines A549, NCI-H2009 and NCI-H358 **(c)** and the UCEC cell line Ishikawa **(d)** in the *MYC* region. **(e)** 3C interaction frequency ± SEM measured by chromosome conformation capture assays (n = 3) in A549 and Ishikawa cells. The 3C 'anchor' primer targets the *MYC*

promoter region, while the 3C 'bait' primers target the non-coding regions 3′ to *MYC*. The *P*-value is derived from a t-test; (**) *p* 0.01; (***) *p* 0.001. **(f)** Left: Log2 transformed expression level (RPKM) of *MYC* in LUAD tumors with focal amplification of either *MYC* alone (n = 7) or *MYC*-LASE alone (n = 11) and tumors without these amplifications (n = 235). Right: UCEC tumors with focal amplification of either *MYC* alone (n = 10) or *MYC*-ECSE (n = 14) and tumors without these amplifications (n = 250). Box plot: Middle bar, median; lower and upper box limits, 25th and 75th percentiles, respectively; whiskers, min and max. The *P*-value is derived from a t-test; (***) *p* 0.001.
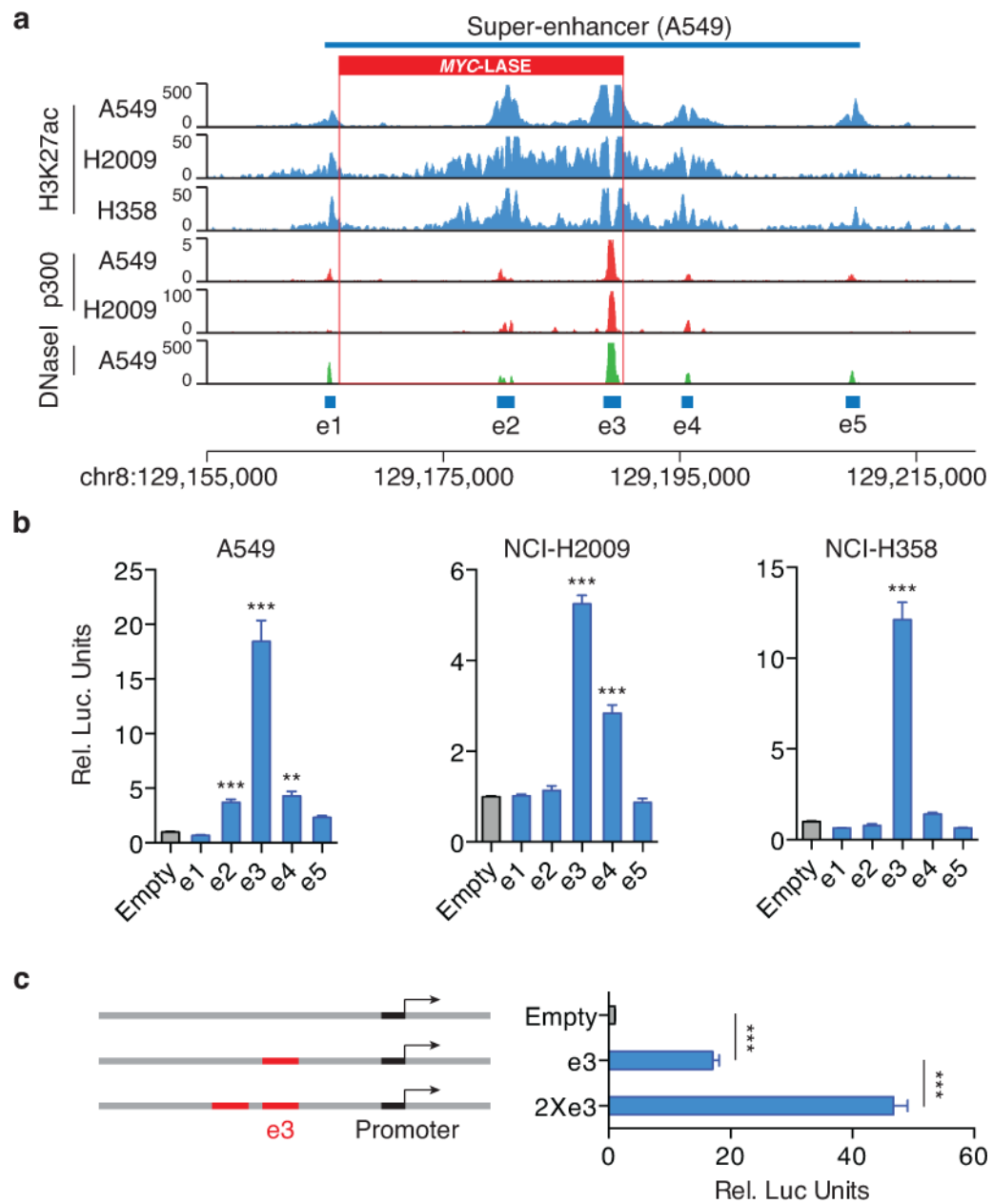
Fig. 3. The activity of the *MYC*-LASE is predominantly driven by the e3 constituent enhancer
(a) H3K27ac, p300 binding and DNase I hypersensitivity profiles in A549, NCI-H2009 and NCI-H358 cells reveal the constituent enhancers e1-e5 within the super-enhancer region. **(b)** Luciferase reporter assay (n = 3) measuring enhancer activity of e1-e5 in A549, NCI-H358 and NCI-H2009 lung adenocarcinoma cells. The pGL3 plasmid without the enhancer region (Empty) is used as a negative control. (*Y*-axis) Relative Luciferase units are normalized to *Renilla* signal ± SEM. The *P*-value is derived from a t-test; (**) *p*   p0.01; (***) *p* 0.001. **(c)** Enhancer activity of a duplicated e3 enhancer (2×e3) ± SEM as measured by luciferase reporter assay (n = 3). The *P*-value is derived from a t-test; (***) *p* 0.001.
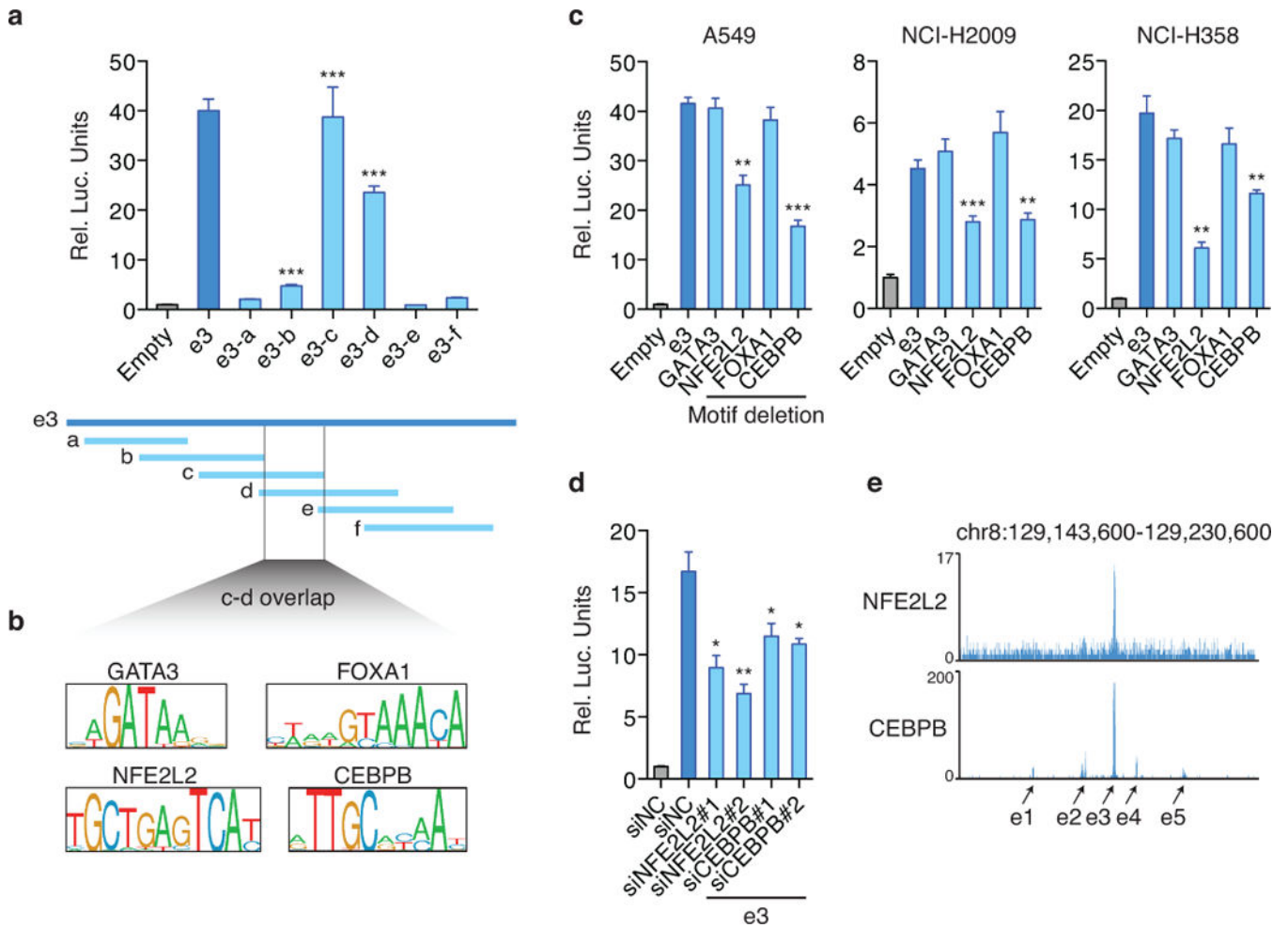
Fig. 4. Identification of transcription factors required for the activity of the e3 enhancer
(a) Enhancer activity ± SEM of small fragments (a-f) of the e3 enhancer as assessed by luciferase reporter assays (n = 3) in A549 LUAD cells. The fragments c and d show comparable enhancer activity relative to the intact e3 enhancer, while other fragments show minimal enhancer activity. The *P*-value is derived from a t-test; (***) p 0.001. (b) Transcription factor DNA recognition motifs are identified in the mini-e3 enhancer region that is defined by the c and d fragments overlap. (c) The luciferase reporter expression level ± SEM after deletion of individual transcription factor motif sequence in the e3 regions. The *P*-value is derived from a t-test (n = 3); (**) p 0.01; (***) p 0.001. (d) Luciferase reporter expression level ± SEM after silencing NFE2L2 or CEBPB by siRNA (n = 3). The *P*-value is derived from a t-test; (*) p 0.05; (**) p 0.01. (e) ChIP-seq profile of NFE2L2 and CEBPB in the e1–e5 enhancer regions in A549 cells.
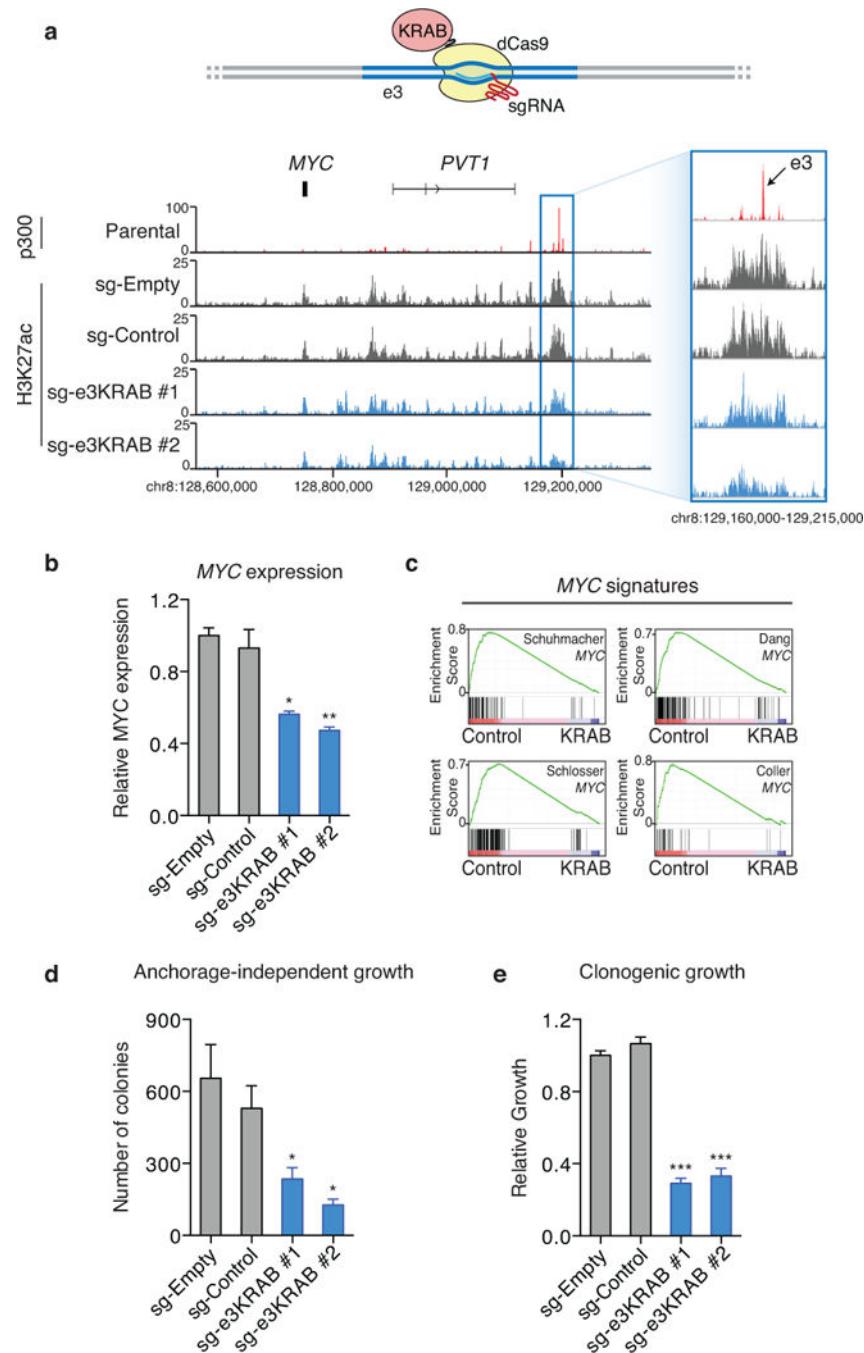
Fig. 5. KRAB-dCas9 mediated repression of the e3 enhancer reveals *MYC* as a direct target
(a) Upper: the design of KRAB-dCas9 mediated repression of the e3 enhancer. Bottom: ChIP-seq of H3K27ac in NCI-H2009 cells with and without KRAB-dCas9 enhancer repression. p300 ChIP-seq profile in parental NCI-H2009 cells indicates the e3 enhancer region. sg-Empty: no sgRNA; sg-Control: sgRNA that is predicted to not recognize any genomic regions; sg-e3KRAB #1 and sg-e3KRAB #2: two separate sgRNAs recognizing the e3 enhancer region. **(b)** The expression level of *MYC* ± SEM as measured by quantitative PCR in NCI-H2009 cells with and without KRAB-dCas9 mediated repression of the e3

enhancer (n = 2). **(c)** GSEA analysis of RNA-seq data generated in NIC-H2009 cells with and without KRAB-dCas9 mediated e3 enhancer repression reveals that genes regulated by e3 repression are enriched in *MYC* target genes identified by previous studies[44–47]. The cellular transformation efficiency ± SEM as measured by anchorage-independent growth (n = 3) **(d)** and the cellular proliferation rate ± SEM as measured by clonogenic assays (n = 3) **(e)** in NCI-H2009 cells with and without KRAB-dCas9 mediated repression of the e3 enhancer. The *P*-value is derived from a t-test; (*) *p* 0.05; (**) *p* 0.01; (***) *p* 0.001.
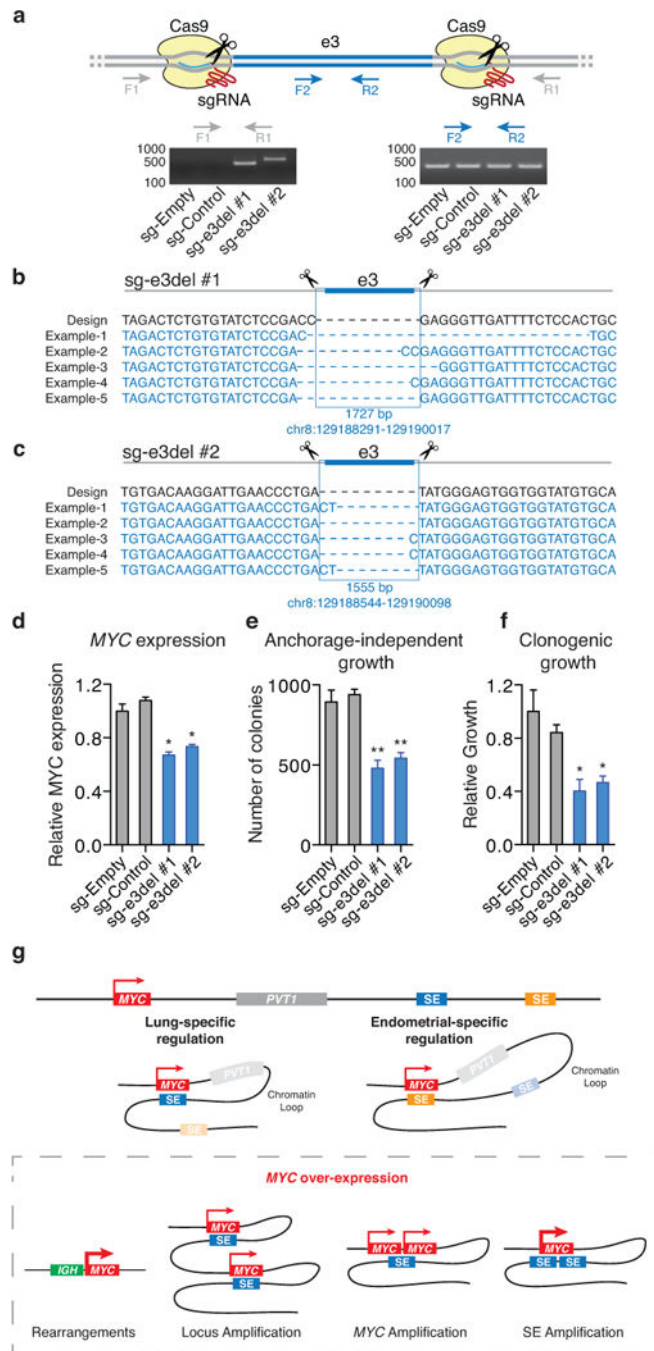
Fig. 6. CRISPR/Cas9 mediated deletion of the e3 enhancer impairs the oncogenic effect of the e3 enhancer amplification

(a) Upper: design of CRISPR/Cas9 mediated deletion of the e3 enhancer. Primers used to validate the e3 enhancer deletion are indicated. Bottom: Gel pictures of PCR amplification of genomic DNA using primers outside and inside the e3 enhancer region. sg-Empty: no sgRNA; sg-Control: a pair of sgRNAs that are predicted to not recognize any genomic regions; sg-e3del #1 and sg-e3del #2: two separate pairs of sgRNAs recognizing boundaries of the e3 enhancer region. PCR products were cloned into individual vectors and sequenced.

Sequencing results represent the deletions induced by sg-e3del #1 **(b)** and sg-e3del #2 **(c)**. The expression level of MYC ± SEM as measured by quantitative PCR (n = 2) **(d)**, the cellular transformation efficiency ± SEM as measured by anchorage-independent growth (n = 3) **(e)** and the cellular proliferation rate ± SEM as measured by clonogenic assays (n = 3) **(f)** in NCI-H2009 cells with and without CRISPR/Cas9 mediated deletion of the e3 enhancer. The P-value is derived from a t-test; (*) p 0.05; (**) p 0.01. **(g)** Schematic representation of genomic structural variants activating MYC expression in cancer.